PAPER Special Issue on Recent Progress in Electromagnetic Compatibility Technology

Calculation of Temperature Rises in the Human Eye Exposed to EM Waves in the ISM Frequency Bands

Akimasa HIRATA†, *Student Member*, **Gou USHIO**†, *Nonmember*, *and* **Toshiyuki SHIOZAWA**†, *Member*

SUMMARY The interaction between the human eye and electromagnetic (EM) waves in the ISM (industrial, scientific, and medical) frequency bands is investigated with the use of the finite-difference time-domain (FDTD) method. In order to assess possible health hazards, the specific absorption rates (SARs) are calculated and compared with the recommended safety standards. In particular, we calculate temperature rises in the human eye to assess the possibility of microwave-induced cataract formation. The results show that the maximum values of averaged SARs are less than the standard levels. In addition, we observed what is called the 'hot spot' in the region of eye humor at 2.4 GHz but not at 900 MHz and 5.8 GHz. Furthermore, the maximum temperature rise due to the incident EM power density of 5.0 mW/cm^2, which is the MPE (maximum permissible exposure) limit for controlled environments, has been found to be at most 0.26°C at 5.8 GHz, which is small compared with the threshold temperature rise 3.0°C for cataract formation.

key words: *FDTD method, human eye, ISM frequency bands, specific absorption rate (SAR), temperature rise*

1. Introduction

In recent years, there has been an increasing public concern about possible health hazards due to exposure to EM waves. Accordingly, many international protection organizations and regulatory agencies have proposed the safety standards for exposure to EM waves [1]–[4]. These standards are based on the SAR, which is a measure of the EM power absorbed in the tissue. Thus a great deal of theoretical work has been done on the SAR distributions in human bodies for exposure to EM waves, assessing possible health hazards based on these standards (reviewed in Ref. [5]).

The ISM frequency bands (900 MHz, 2.4 GHz, and 5.8 GHz bands) [6] assigned for multiple-user applications are suitable for, and expected for, the wireless LAN applications. The applications typically support a limited number of users in an indoor area. Thus the users are unconsciously exposed to EM waves which directly come from antennas or which are reflected and scattered from objects existing in the area [7]. The applications in these frequency bands also include portable telephones, microwave ovens, and so forth. The purpose of this paper is to investigate the thermal distributions in the human eye exposed to EM waves in the ISM frequency bands. The reason for focusing our discussion on the human eye is that it seems to be one of the most hazardous organs because it has neither blood flow to carry away the heat evolved nor skin layer to protect it [8]–[10]. In the previous papers, the calculations have been carried out at 750 MHz [8], 1.5 GHz [8], [9], and 6–30 GHz [10]. The dielectric properties of human tissues, however, are frequency-dependent [11], [12]. Therefore, the SAR distributions in the human eye should depend on the frequencies of applied EM fields. This is the important fact to stress. In this paper, we discuss in detail the frequency dependence of SAR distribution for the human eye in the ISM frequency bands.

Additionally, we calculate the temperature rise in the human eye by using the Pennes' bioheat equation [13] for investigating the possibility of microwave-induced cataract formation [14], [15].

2. FDTD Method and Model for the Analysis

In this paper, we investigate the thermal distributions in an anatomically-based model of the human eye exposed to the EM wave in the ISM bands, with the use of the FDTD method. The procedures for constructing the model for the analysis are largely dependent on Ref. [10]. In addition, only the outline of the FDTD method will be described, since the detailed account of the method can be found in the literature [16]–[18].

2.1 The Model of the Human Eye

In this paper, we do not consider a whole–head model but a model which only consists of the eye and the surrounding head region [8]–[10]. However, we have to obtain reasonable solutions even if we use a simplified model. For this purpose, we consider a two-dimensional human head model as shown in Fig. 1. Note that the procedures for constructing the model will be described later in this section. We also consider another model in which the rear part of the head is removed along the line (A–A' in Fig. 1). The position of this line is chosen so that a sufficient portion of brains is included in the model to get reasonable numerical results. The validity of this model is guaranteed by the following facts:

Manuscript received June 30, 1999.
Manuscript revised September 27, 1999.

†The authors are with the Department of Communication Engineering, Graduate School of Engineering, Osaka University, Suita-shi, 565-0871 Japan.

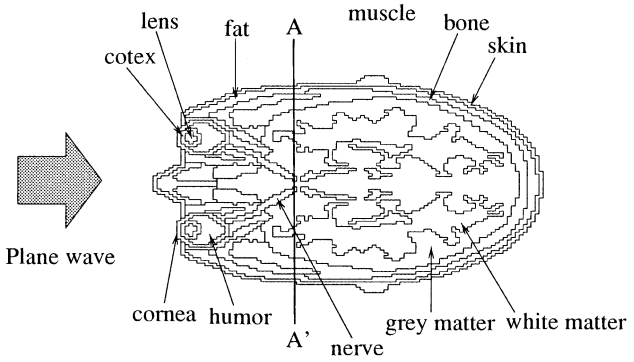

Fig. 1 Two-dimensional human head model through the center of the eye.

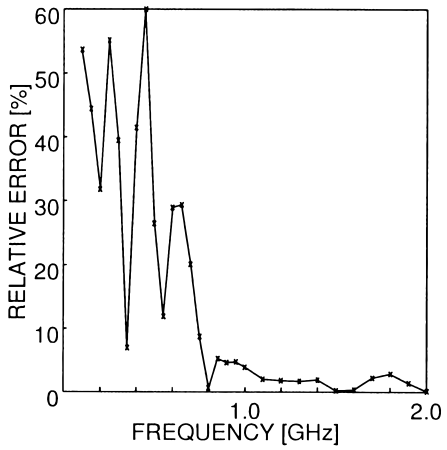

Fig. 2 Relative errors in the SARs averaged over the human eye.

- Major reflections occur at the boundaries between eyeball and fat, and at those between fat and brains. Therefore, the transmitted waves to brains are not so large.
- The transmitted wave to brains is damped to be small enough due to the conductivity of the tissue. Hence, the SAR in the human eye is not affected so much by the reflected wave from the back ends of the human head.

Then, these models are illuminated by a plane wave from the front of the head model. We calculate the SARs averaged over the human eye for these two models and compare them in the frequency range between 0.1 GHz and 2.0 GHz. We show in Fig. 2 the relative errors of averaged SARs between the two models. As seen from Fig. 2, the relative errors of averaged SARs are not so large, i.e., within 5.0% in the frequency range above 800 MHz. The reason why the relative errors are large below 800 MHz is that the conductivities of tissues are not so large. Fortunately, the frequency range we treat in this paper is above 800 MHz. Thus we construct the human eye model with the aid of a simplified model in which the rear part of the head is removed.

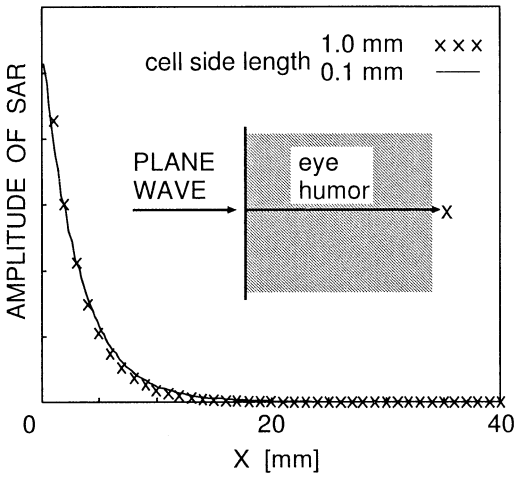

Fig. 3 SAR distributions in the semi-infinite eye humor. (The amplitude of SAR is arbitrary.)

The human eye model has been constructed from photographic images of the human head. These images whose resolution is 3 dots / mm have been taken from the Internet site "The Visible Human Project"(http://www.nlm.nih.gov/research/visible/visible_human.html). In order to use these images in the FDTD method, we must divide them into cells. In this paper, we divide these images into cubic cells with its side length of 1.0 mm. We should notice that the FDTD stability requires cell dimensions less than $\lambda_\epsilon/10$, where λ_ϵ is the shortest wavelength in the system to be considered. We must use the cells with its side length of about 0.7 mm at 5.8 GHz in order to satisfy this condition strictly. For comparison, we show in Fig. 3 the SAR distributions in the semi-infinite layer of eye humor for the cubic cell with its side length of 0.1 mm and 1.0 mm. Note that the results with the use of 0.1 mm cell corresponds to a more accurate solution, because the condition mentioned above is well satisfied. As seen from Fig. 3, we could obtain good agreement with the accurate solution even if we use the cell size of 1.0 mm. Thus, in this paper, we use the cubic cells with its side length of 1.0 mm. The main reason for the validity of this simplification is that the eye humor is a highly lossy medium in the frequency range above a few GHz [12]. Similar results of SAR calculations are reported in Refs. [10], [19].

For geometries in which the wave-object interaction has to be considered in open regions, the computational space has to be truncated by using absorbing boundary conditions (ABC) (See Refs. [16], chap.7 and [18], chap.2). In this paper, we adopt the Mur's 2nd order ABC. In our simulation, we do not use the whole head model but use a simplified human head model which has been specified in the foregoing discussion. Therefore, the model abuts on the boundary at the planes z=−22, z=58, and y=80 [mm]. Thus,

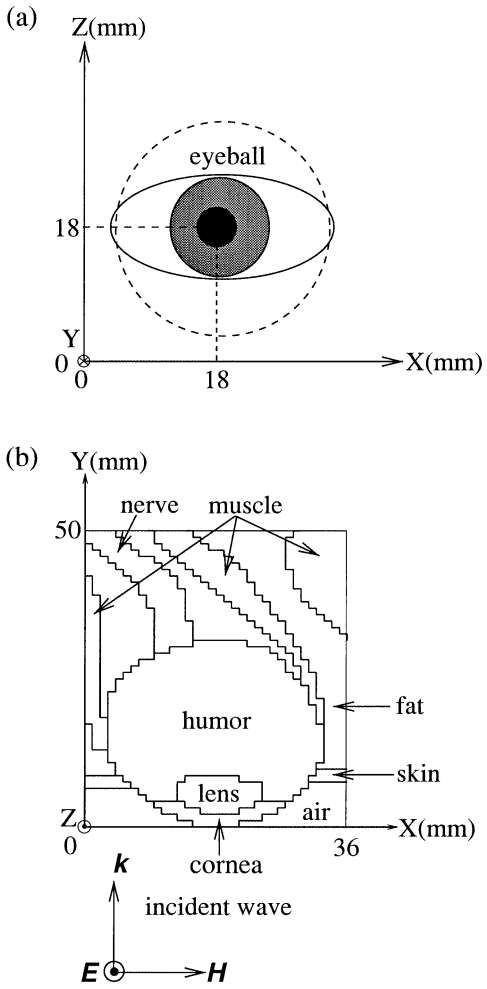

Fig. 4 Geometry of the Problem. (a) Front view of the human eye image. (b) Top view of the model around the eyeball on the horizontal plane ($z = 18$ [mm]).

at the planes z=−22 and 58 [mm], which is parallel to the propagation direction of the incident wave, we have made the absorbing boundaries (ABs) themselves involve conductivities for avoiding unphysical wave propagations. Note that the conductivities of tissues chose to ABs are used for those of ABs. The reflections at the boundary are not negligible, but they do not affect the human eye so much. On the other hand, the symmetric boundary condition is applied along the center of the nose.

The model obtained above is shown in Fig. 4, with the coordinate system. Figures 4(a) and (b) show, respectively, the front view of the human eye image and the top view of the model around the eyeball on the horizontal plane ($z = 18$ [mm]). The model obtained is comprised of $80 \times 80 \times 80$ cells. In this model, the eye occupies a volume of 10.9 cm^3, corresponding to a mass of 11.0 g.

Table 1 Dielectric properties of the human tissues in the ISM frequency bands.

Freq.	900 MHz		2.4 GHz		5.8 GHz	
Tissues	ϵ_r	σ	ϵ_r	σ	ϵ_r	σ
skin	46.1	0.84	42.9	1.56	38.6	4.34
fat	11.3	0.11	10.8	0.26	9.86	0.83
brains†	45.8	0.77	42.6	1.48	38.3	4.24
humor	68.9	1.64	68.2	2.44	64.8	6.67
cornea	55.2	1.39	51.7	2.26	46.5	5.66
lens	35.8	0.48	34.0	1.06	30.5	3.43
muscle	56.0	0.97	53.6	1.77	49.0	5.20
nerve	32.5	0.57	30.2	1.07	27.2	2.94

† The dielectric constants averaged over white matter and grey matter are used for those for brains.

2.2 Dielectric Properties of Tissues

In the last subsection, we have constructed the human eye model composed of nine tissues, i.e., lens, cornea, humor, nerve, fat, skin, bone, brains, and muscle. In order to incorporate these tissues into the FDTD method, we must have their dielectric properties. The dielectric properties of the tissues are determined with the aid of the 4-Cole-Cole extrapolation [12]. The dielectric properties of the tissues in the ISM frequency bands are listed in Table 1.

3. SAR Calculations

We give, at the initial state, a plane wave [16] with vertical polarization (See Fig. 4(b)). The power density for the EM wave is assumed to be $P_0 = 5.0\,[\mathrm{mW/cm^2}]$, which is the value of MPE limit for controlled/occupational environments. Note that this value is slightly different on the guidelines and/or in frequency ranges [1]–[4]. On the other hand, according to the IEEE 802.11 wireless LAN standard, the maximum permitted output power of antennas for wireless LAN applications at 2.4 GHz is 1.0 [W] in the United States, 0.10 [W] in Europe, and 10 [mW/MHz] in Japan. Then, the power density 5.0 [mW/cm^2], needless to say, would be sufficiently larger than the worst exposure for uncontrolled/public environments. Hence, the results obtained in our simulation would cover various situations.

3.1 Calculations of SAR Distributions

For harmonically varying EM fields, the SAR is defined as

$$\mathrm{SAR} = \frac{\sigma}{2\rho}|\hat{E}|^2 = \frac{\sigma}{2\rho}(|\hat{E}_x|^2 + |\hat{E}_y|^2 + |\hat{E}_z|^2), \quad (1)$$

where $\hat{E}_x$, $\hat{E}_y$, and $\hat{E}_z$ are the peak values of the electric field components.

First, we show in Fig. 5 the SAR distributions on the horizontal plane ($x = 18$ [mm]). As seen from Fig. 5, the SAR distributions greatly depend on the frequencies of the incident wave. For higher frequencies, the

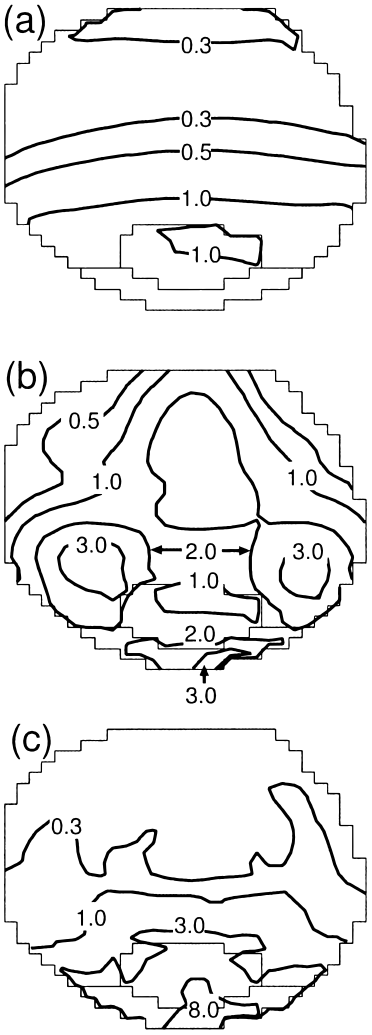

Fig. 5 SAR distributions on the horizontal plane ($z = 18$ [mm]) at (a) 900 MHz, (b) 2.4 GHz, and (c) 5.8 GHz.

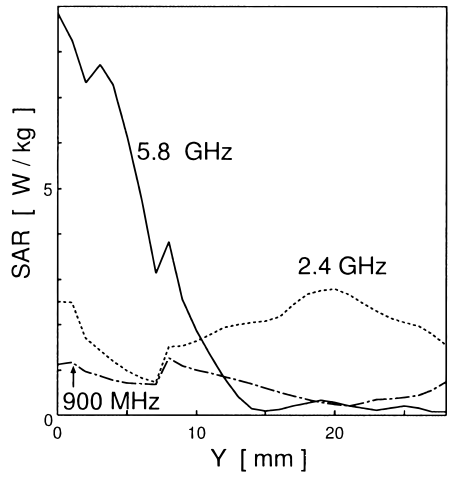

Fig. 6 SAR distributions along the line ($x = z = 18$ [mm]).

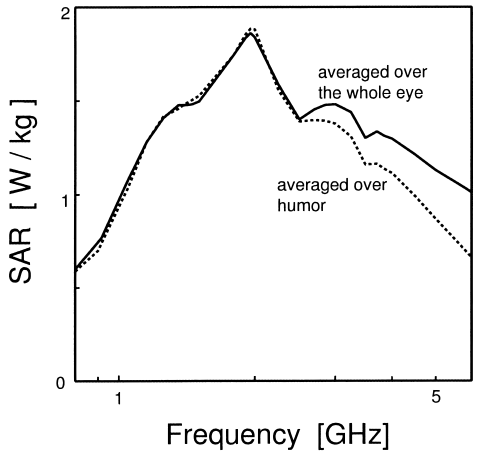

Fig. 7 Dependence of the averaged SAR on the frequencies of incident wave ($P_0 = 5.0$ [mW/ cm^2]).

peak values of local SARs are larger and the SAR distributions are concentrated around lens and cornea. The main reason for this is that the conductivities of tissues become larger as frequency is increased [11], [12], resulting in the decrease of the penetration depth of EM fields. In order to clarify the EM penetration in the eye, we illustrate in Fig. 6 the spatial distributions of the SAR along the center line of the eye. Note in Fig. 6 that the regions of 0–2.0 [mm], 2.0–9.0 [mm], and 9.0–28 [mm] correspond, respectively, to cornea, lens, and humor. As seen from Fig. 6, the SAR distribution at 5.8 GHz is concentrated around cornea and steeply drops as we move into the interior of the eye. This is because the penetration depth of EM fields becomes shorter at 5.8 GHz, as mentioned before. Additionally, what is called the 'hot spot' is observed in the region of eye humor at 2.4 GHz ($z \simeq 16$ [mm]) but not at 900 MHz and 5.8 GHz. It is not easy to explain this difference in short. Thus, we investigate how the SAR distribution depends on the frequencies of the incident wave.

We show in Fig. 7 the dependence of the SARs averaged over the whole eye and those averaged over the humor on the frequencies of the incident wave. In this analysis, we carry out numerical simulations in the frequency range between 800 MHz and 6 GHz. As is evident from Fig. 7, both the averaged values of SARs become maximum around 1.9 GHz, which corresponds to resonance. Similarly, both the averaged SARs have two slight peaks at 2.9 GHz and 3.7 GHz. Then, the frequency 2.4 GHz is located between these resonant frequencies and the eye becomes a quasi-resonant structure there. This is evident from Fig. 5(b) where the SAR is substantially distributed over the whole eye. Hence, the hot spot is found to be closely associated with geometrical resonance. On the other hand, the wavelength at 900 MHz is larger than the fundamental resonant wavelength. Therefore, the SAR distributions are not largely affected by the geometrical structure of the eye. At 5.8 GHz, as mentioned before, the SAR

Table 2 Comparison of averaged SAR values in W/kg.

1.5 GHz	1g peak	whole eye
Our Results	1.98	1.24
Results in [9]	2.11	1.22
6.0 GHz	1g peak	whole eye
Our Results	3.12	1.20
Results in [10]	–	1.25

distribution is concentrated around cornea and lens. This phenomena is also evident from Fig. 7 where the difference between the SAR averaged over humor and that averaged over the whole eye becomes larger as frequency is increased in the range above 4 GHz.

As stated before, this paper focuses on the thermal distributions in the eye for plane wave exposures in the ISM bands. In particular, resonance phenomena found in this paper come from the standing waves due to the geometrical structure of the eye. A more detailed account of resonances in the eye is shown in Ref. [20].

Finally, in order to confirm the validity of our results, we compare our results with those reported in [9] at 1.5 GHz and with those reported in [10] . In these comparisons, we use the dielectric constants in each reference and adjust the size of our model to that reported in each reference. As is evident from Table 2, our results coincide with those reported before. Slight differences in the compared results would mainly come from the difference in the modeling of the human eye. Note that in Table 2 '1g peak' corresponds to the maximum value averaged over 1g tissues ($10 \times 10 \times 10$ cells). Thus one can safely state that the accuracy of our model fall within an acceptable range.

3.2 Comparison of the Calculated Data with the Safety Standards

We compare the SARs obtained in our simulation with the safety standards [1]–[4]. According to the guidelines approved by CENELEC (1995) [2], the Ministry of Posts and Telecommunications (1997) [3], and ICNIRP(1998) [4], exposure conditions are acceptable if it can be shown that peak SAR values averaged over any 10 g tissue and over the time duration of 6 minutes are less than 10 W/kg[†] for controlled environments. According to IEEE/ANSI [1], on the other hand, the standard is based on the peak SAR value averaged over any 1 g tissue (in the shape of a cube), and it must be less than 8 W/kg for controlled environments.

We show in Table 3 the SAR values averaged over 1g tissues and the whole eye. Note that, in this paper, we adopt the SAR values averaged over the whole eye (11.0 g) as those averaged over 10 g tissues.

The SARs averaged over the whole eye at 900 MHz, 2.4 GHz, and 5.8 GHz are, respectively, 0.77, 1.45, and 1.03 [W/kg]. These values are much less than 10 W/kg, which means that they are within the safety standards. For the SARs averaged over 1 g tissue as well, the values obtained in our simulation are less than the safety standards. Thus local peak SARs for the worst exposure in the ISM frequency bands are well within the safety standards, as far as the human eye is concerned.

Table 3 SAR values averaged over tissues in W/kg.

	915 MHz	2.4 GHz	5.8 GHz
1g peak	1.11	2.72	3.03
Whole eye	0.77	1.45	1.03

4. Temperature Calculations

In this section, we calculate the temperature rises due to the microwave heating in the human eye in order to assess the possibility of microwave-induced cataract formation, with the use of the Pennes' bioheat equation [13]. When the thermal problem associated with the eye is considered, the following simplifications are valid [10], [22]. First, the blood flow in the human eye is absent. Secondly, the heat exchange between the human eye and surrounding tissues are negligible. Thus the human eye is considered as the object thermally isolated from the head.

4.1 Bioheat Equation and Thermal Parameters

For calculating the temperature rises in the human eye, we use the Pennes' bioheat equation [13], [21]:

$$C_t \rho_t \frac{dT}{dt} = K\nabla^2 T - \rho_t(\mathrm{SAR}) - b_t T \tag{2}$$

where T denotes the temperature rise of the tissue, K the thermal conductivity of the tissue, C_t the heat capacity of the tissue, and b_t the term associated with blood flow. Note that in this analysis as mentioned above, the term b_t is negligible. Additionally, the boundary condition for Eq. (2) is given in the next equation [8], [10], [22], [23],

$$H \cdot (T_s - T_e) = -K\frac{\partial T}{\partial n} \tag{3}$$

where H, T_s, and T_e denote, respectively, the convection coefficient, the surface temperature, and the fluid temperature (corresponding to air and body core temperatures).

We show in Table 4 the thermal parameters of human tissues. In this paper, we use the thermal parameters of water as those for cornea and the heat capacity of humor, as well as in Refs. [10], [22]. Note that the thermal parameters for cornea may not be close to those of humor. However, this mismatch does not lead to obvious errors, because the volume of cornea is very small. Additionally, we use 20 [W/m^2·°C] and 65 [W/m^2·°C] as the value of the convection coefficient between the eye surface and air H_1 and that between the eye surface

[†]The shape of 10 g tissue is a cube in CENELEC.

Table 4 Thermal parameters of the Human Tissues.

Tissues	C_t [J/kg·°C]	K [W/m· °C]
Cornea	4178	0.603
Humor	4178	0.59†
Lens	3000‡	0.40‡

† [24]. ‡[25]. The other parameters are assumed to be equal to those of water.

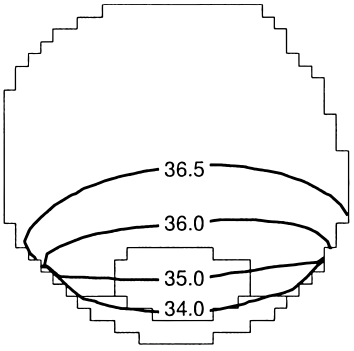

Fig. 8 Temperature distribution at the initial state ($z = 18$ [mm]).

and body core H_2, respectively [22]. We should notice that the value of H_1 includes the following effects, i.e., *i)* evaporation of the tear film, *ii)* convective exchange with the air, and *iii)* radiative exchange with the surrounding objects. Furthermore, this value is obtained in the condition where the room temperature is 23°C. Thus, in this paper, the room temperature is assumed to be 23°C. On the other hands, the body core temperature is assumed to be 37°C.

We should notice that the results based on animal experiments are used for the thermal parameters of humor and lens in this paper, because we have no reliable data available on the parameters required in the model of the human eye. Additionally, the thermal parameters of water are used as those for cornea and the heat capacity of humor, as mentioned above. Therefore, the following results would clearly involve some uncertainties.

4.2 Temperature Rises

At the initial state, we give the temperature distribution for steady-state as shown in Fig. 8. This distribution is obtained from the steady-state bioheat equation [22]

$$K\nabla^2 T = 0 \tag{4}$$

subject to the boundary conditions (Eq. (3)). Here, the distribution is not symmetrical. This is mainly caused by the geometrical asymmetry of the eye, particularly by that of the eyelid.

We show in Fig. 9 the temperature rises along the center line of the eye. From Fig. 9, the peak temperature rise in the eye is, respectively, 0.09°C at 900 MHz,

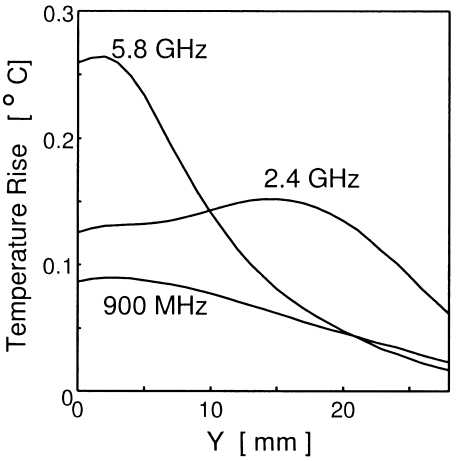

Fig. 9 Temperature rises along the line ($x = z = 18$ [mm]).

0.15°C at 2.4 GHz, and 0.26°C at 5.8 GHz. Note that this temperature rises are caused by EM exposures with power density of 5.0 [mW/cm^2], because the SAR distributions are calculated at that power density.

Comparing Figs. 6 and 9, the distributions of temperature rise are not linearly proportional to those of SAR. The reason for this is that the heat in the human body is diffused by Eq. (2). Additionally, the temperature rises are relatively concentrated around the region of lens. The reason for this is that the convection coefficient between human eye and air H_1 is small compared with those between the human eye and the human head H_2, leading to the heat concentration around lens. The temperature rise for exposure to EM waves in the ISM bands was at most 0.26°C at 5.8 GHz, which is found to be small compared with the threshold temperature rise 3.0°C for cataract formation [14].

5. Conclusions

In this paper, the thermal distributions in the human eye for plane wave exposures in the ISM frequency bands were evaluated. For the analysis of the problem, we constructed an anatomically-based model, and the interaction between the model and the EM waves were investigated with the aid of the FDTD method. First, the SAR distributions were calculated in the model and compared with the recommended safety standards. Additionally, for assessing the possibilities of microwave-induced cataract formation, we calculated the temperature rises in the human eye for exposure to EM waves with power density 5.0 [mW/cm^2], which is the MPE limit for controlled environments.

From numerical analysis, we found the following results. The SAR distributions were found to be greatly dependent on the frequencies of the incident wave. Secondly, the SARs averaged over 10 g tissues were found to be small compared with the recommended standards. Furthermore, the maximum temperature rise for expo-

sure to EM waves in the ISM bands was at most 0.26°C at 5.8 GHz, which is found to be small enough compared with the threshold temperature rise 3.0°C for cataract formation.

Acknowledgement

The authors would like to thank T. Katayama and S. Matsuyama (Graduate school of engineering, Osaka University) for their useful discussions.

References

[1] IEEE C95.1–1991 IEEE standard for safety levels with respect to human exposure to radio frequency electromagnetic fields, 3 kHz to 300 GHz, IEEE, Inc., New York, 1992.
[2] European Committee for Electrotechnical Standardization (CENELEC) Prestandard ENV 50166, Human exposure to electromagnetic fields. High frequency (10 kHz to 300 GHz), Jan. 1995.
[3] "Radio-radiation protection guidelines for human exposure to electromagnetic fields," Telecommun. Technol. Council Ministry Posts Telecommun, Deliberation Rep. 89, Tokyo, Japan, 1997.
[4] ICNIRP Guidelines, "Guidelines for limiting exposure to time-varying electric, magnetic, and electromagnetic fields (up to 300 GHz)," Health Phys., vol.74, pp.494–522, 1998.
[5] M.A. Stuchly, "Biomedical concerns in wireless communications," Crit. Rev. Biomed. Eng., vol.26, pp.117–151, 1998.
[6] F. Ali and J.B. Horton, "Introduction to the special issue on emerging commercial and consumer circuits, systems, and their applications," IEEE Trans. Microwave Theory & Tech., vol.43, no.7, pp.1633–1637, Oct. 1995.
[7] K. Pahlavan and A.H. Levesque, "Wireless data communications," Proc. IEEE, vol.82, pp.1398–1430, 1994.
[8] A. Taflove and M.E. Brodwin, "Computation of the electromagnetic fields and induced temperatures within a model of the microwave-irradiated human eye," IEEE Trans. Microwave Theory & Tech., vol.23, no.11, pp.888–896, 1975.
[9] O. Fujiwara and A. Kato, "Computation of SAR inside eyeball for 1.5-GHz microwave exposure using finite-difference time-domain technique," IEICE Trans. Commun., vol.E77-B, no.6, pp.732–737, June 1994.
[10] P. Bernardi, M. Cavagnaro, S. Pisa, and E. Piuzzi, "SAR distribution and temperature increase in an anatomical model of the human eye exposed to the field radiated by the user antenna in a wireless LAN," IEEE Trans. Microwave Theory & Tech., vol.46, no.12, pp.2074–2082, 1998.
[11] C.C. Johnson and A.W. Guy, "Nonionizing electromagnetic wave effects in biological materials and systems," Proc. IEEE, vol.60, pp.692–718, 1972.
[12] C. Gabriel, "Compilation of the dielectric properties of body tissues at RF and microwave frequencies," Final Technical Report Occupational and Environmental Health Directorate AL/OE-TR-1996-0037 (Brooks Air Force Base, TX: RFR Division).
[13] H.H. Pennes, "Analysis of tissue and arterial blood temperature in resting forearm," J. Appl. Physiol., vol.1 pp.93–122, 1948.
[14] A.W. Guy, J.C. Lin, P.O. Kramar, and A. Emery, "Effect of 2450-MHz radiation on the rabbit eye," IEEE Trans. Microwave Theory & Tech., vol.23, no.6, pp.492–498, 1975.
[15] Y. Kamimura, K. Saito, T. Saiga, and Y. Amemiya, "Effect of 2.45 GHz microwave irradiation on monkey eyes," IEICE Trans. Commun., vol.E77-B, no.6, pp762–765, June 1994.
[16] A. Taflove, Computational Electrodynamics: The Finite-Difference Time-Domain Method, Artech House, Norwood, MA, 1995.
[17] O.P. Gandhi, "Some numerical methods for dosimetry: Extremely low frequencies to microwave frequencies," Radio Sci., vol.30, no.1, pp.161–177, 1995.
[18] T. Uno, Finite Difference Time Domain Method for Electromagnetic Field and Antenna Analysis, Corona, Tokyo, 1998.
[19] O.P. Gandhi, Y.G. Gu, J.Y. Chen, and H.I. Bassen, "SAR and induced current distributions in a high-resolution in anatomically based model of a human for plane-wave exposures 100–915 MHz," Health Phys., vol.63, pp.281–290, 1992.
[20] G. Ushio, A. Hirata, and T. Shiozawa, "Formation of hot spots in the human eye," IEICE Trans., vol.J82-B, pp.1605–1607, 1999.
[21] K.R. Foster, A. Lozano-Nieto, and P.J. Riu, "Heating of tissues by microwaves: A model analysis," Bioelectromagnetics, vol.19, pp.420–428, 1998.
[22] J.A. Scott, "A finite element model of heat transport in the human eye," Phys. Med. Biol., vol.33, pp.227–241, 1988.
[23] O. Fujiwara, M. Yano, and J. Wang, "FDTD computation of temperature-rise inside realistic head model for 1.5 GHz microwave exposure," IEICE Trans., vol.J81-B-II, no.3, pp.240–247, 1998.
[24] H. Pauly and H.P. Schwan, "The dielectric properties of the bovine eye lens," IEEE Trans. Bio-Med. Eng., vol.11, pp.103–109, 1964.
[25] J.J.W. Lagendijk, "A mathematical model to calculate temperature distributions in human and rabbit eyes during hyperthermic treatment," Phys. Med. Biol., vol.27, pp.1301–1311, 1982.

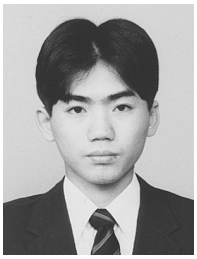

Akimasa Hirata was born in Okayama, Japan, on November 27, 1973. He received the B.E. and M.E. degrees in electrical communication engineering from Osaka University, Osaka, Japan, in 1996 and 1998, respectively. He is currently pursuing the Ph.D. degree at Osaka University. His research interests are numerical simulation on free-electron lasers and bioelectromagnetics. He is a recipient of the presentation award for young scientists from IEEJ (Institute of Electrical Engineers of Japan) in 1998 and also a research fellow of the Japan Society for the Promotion of Science (JSPS Research Fellow). Mr. Hirata is a student member of IEEE.

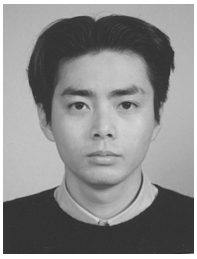

Gou Ushio was born in Hyogo, Japan, on April 24, 1972. He received the B.E. and M.E. degrees in communication engineering from Osaka University, Suita, Osaka, Japan, in 1997 and 1999, respectively. He was engaged in the study of bioelectromagnetics while he was at the graduate school of Osaka University. He is now working at Kansai Electric Power Corporation.

Toshiyuki Shiozawa was born in Tokyo, Japan, on January 16, 1941. He received the B.E., M.E., and Ph.D. degrees in electrical communication engineering from Osaka University, Suita, Osaka, Japan, in 1964, 1966, and 1969, respectively. In 1969, he joined the Department of Communication Engineering, Osaka University, where he is now a Professor. He has been engaged in the research of relativistic electromagnetic theory for engineering-oriented applications, and free-electron lasers in the millimeter and submillimeter wave regions. His current research interests include nonlinear electromagnetics and bioelectromagnetics. He has been serving as a member of the Editorial Boards of the IEEE Transactions on Microwave Theory and Techniques and the Journal of Applied Physics. He served also as an Associate Editor of the IEICE Transactions on Electronics from 1995 to 1999. He is the Chairman of the Technical Committee on Electromagnetic Theory in IEE Japan (Institute of Electrical Engineers of Japan). He is a co-author of the books *Topics in Advanced Electromagnetic Theory* (Tokyo, Japan: Corona, 1988) and *Exercise in Electromagnetic Theory* (Tokyo, Japan: Corona, 1998). Dr. Shiozawa is a member of the Institute of Electrical Engineers of Japan and a senior member of the IEEE.